A TRANSIONOSPHERIC COMMUNICATION CHANNEL MODEL

By: E. J. FREMOUW   C. L. RINO   A. R. HESSING   V. E. HATFIELD

Prepared for:

ROME AIR DEVELOPMENT CENTER
GRIFFISS AIR FORCE BASE
ROME, NEW YORK   13441
Attn: Mr. Richard A. Schneible
       (OCSE)

CONTRACT F30602-75-C-0236

Sponsored by

STANFORD RESEARCH INSTITUTE
Menlo Park, California 94025 · U.S.A.

AD A127056

DTIC
SELECTED
APR 8 1983

A

83 04 07 10.6

STANFORD RESEARCH INSTITUTE

Menlo Park, California 94025 · U S A

A TRANSIONOSPHERIC COMMUNICATION CHANNEL MODEL

By: E. J. FREMOUW   C. L. RINO   A. R. HESSING   V. E. HATFIELD

Copy No. ....6.

SECURITY CLASSIFICATION OF THIS PAGE (When Data Entered)

REPORT DOCUMENTATION PAGE	READ INSTRUCTIONS BEFORE COMPLETING FORM

1. REPORT NUMBER	2. GOVT ACCESSION NO. *AI27056*	3. RECIPIENT'S CATALOG NUMBER

4. TITLE (and Subtitle) A TRANSIONOSPHERIC COMMUNICATION CHANNEL MODEL	5. TYPE OF REPORT & PERIOD COVERED Quarterly Technical Report 7 Covering the Period 15 May 1977 to 15 July 1977
	6. PERFORMING ORG. REPORT NUMBER SRI Project 4259

7. AUTHOR(s) Edward J. Fremouw Charles L. Rino Anne R. Hessing V. Elaine Hatfield	8. CONTRACT OR GRANT NUMBER(s) Contract F30602-75-C-0236

9. PERFORMING ORGANIZATION NAME AND ADDRESS Stanford Research Institute Menlo Park, California 94025	10. PROGRAM ELEMENT, PROJECT, TASK AREA & WORK UNIT NUMBERS ARPA Order No. 2777

11. CONTROLLING OFFICE NAME AND ADDRESS Defense Advanced Research Projects Agency 1400 Wilson Boulevard Arlington, Virginia 22209	12. REPORT DATE July 1977	13. NO. OF PAGES 50
	15. SECURITY CLASS. (of this report) UNCLASSIFIED	

14. MONITORING AGENCY NAME & ADDRESS (if diff. from Controlling Office) Rome Air Development Center Griffiss Air Force Base New York 13441	15a. DECLASSIFICATION/DOWNGRADING SCHEDULE N/A

16. DISTRIBUTION STATEMENT (of this report)

APPROVED FOR PUBLIC RELEASE
DISTRIBUTION UNLIMITED

17. DISTRIBUTION STATEMENT (of the abstract entered in Block 20, if different from report)

18. SUPPLEMENTARY NOTES

19. KEY WORDS (Continue on reverse side if necessary and identify by block number)

Ionospheric scintillation
Fading
Computer models

20. ABSTRACT (Continue on reverse side if necessary and identify by block number)

This report presents the final results of a three-year contract to develop a signal-statistical model of the transionospheric radio communication channel, building on a previously existing model for first-order signal statistics. The objectives of the contract work were as follows: (1) to test and improve the first-order statistical model; (2) to extend the model to second-order statistical quantities in the temporal, spatial, and spectral domains; (3) to free the model from restriction—

DD FORM 1473
1 JAN 73
EDITION OF 1 NOV 65 IS OBSOLETE

19. KEY WORDS (Continued)

20 ABSTRACT (Continued)

to cases of weak, single scatter; and (4) to calibrate and iteratively test the morphological description of ionospheric structure that underlies the model.

The foregoing objectives have been met, and the research results have been committed to two computer codes for performing systems-oriented, signal-statistical calculations. The more extensive of the two codes, IONSCNT, contains the morphological model and a two-component propagation routine that permits calculation of both focusing and diffractive-scatter effects. Mode I of IONSCNT provides calculation of intensity and phase scintillation indices and other first-order, signal-statistical parameters as functions of frequency, observing geometry, or other relevant variables from a user-selected set of ionospheric state parameters. Mode II of IONSCNT extends the Mode-I results to second-order statistics for cases to be selected by the user. Similarly, the user may employ the second code, DIST, for calculating first-order probability distributions of phase and amplitude (including fade-margin curves) for selected situations.

The model is soundly based in propagation theory and calibrated against the best available scintillation data. It is limited, however, by both theoretical approximations and incomplete data. Inherent in the model are research choices of effective ionospheric scale sizes that probably have no geophysical significance. One result is that the phase scintillation indices calculated account only for the effect of structure of sufficiently small scale (on the order of a kilometer) that intensity scintillation at VHF can be produced. Larger-scale phase trends must be accounted for separately, although a straightforward extrapolation is often adequate. Furthermore, the model describes only representative conditions for the set of input parameters selected by the user. Night-to-night departures from the calculated "mean" scintillation levels for a given set of state parameters (including sunspot number and K_p) are not accounted for and can be considerable.

DD FORM 1 JAN 73 **1473** (BACK)
EDITION OF 1 NOV 65 IS OBSOLETE

CONTENTS

v

ILLUSTRATIONS

I INTRODUCTION

This document presents the final results of an effort to develop a computer model of the transionospheric radio communication channel. It contains an overview of the model, including the propagation theory employed, the ionospheric morphology incorporated, and the signal statistics characterized. Its companion volume (Rino et al., 1977)[*] will be a users' guide to the computer codes developed in the program.

Initial work on the program extended a preexisting model of intensity scintillation to provide a mathematical framework for characterizing the full first-order statistics of a complex signal transmitted through the ionosphere. In the first half of the present contract, the first-order, signal-statistical model was tested against observations of intensity and phase scintillation from the Navy Navigation (Transit) satellites and ATS-6. The model was thereby improved substantially and extended to the second-order, temporal-statistical domain to permit calculation of the temporal autocorrelation functions of intensity and phase. In addition, conditions were removed that had restricted the model to weak, single scatter.

One aspect of recent work on the program was to provide the capability for calculating second-order signal statistics to other than the temporal domain. In particular, one may now employ the computer code IONSCNT to calculate the spatial autocorrelation functions of phase and intensity and the intensity correlation coefficient for two frequencies transmitted through the ionosphere. The final work was to perform iterative testing of the model against definitive intensity and phase scintillation data obtained by means of the DNA Wideband satellite, to improve quantitatively both the signal-statistical and morphological aspects of the model.

---

[*]References are listed at the end of this report.

1

The signal-statistical postulates and the propagation theory employed are described in Section II of this report. The average morphology of the ionospheric structural parameters that control scintillation, as incorporated in the model, is described in Section III. The two computer codes by means of which the model is implemented are outlined in Section IV, and some sample calculations are presented; the codes will be described fully in a companion volume (Rino et al., 1977). It is to be noted that the morphology employed in the model is limited to "average" conditions representative of the ionosphere for a set of state parameters (location, time of day, day of the year, sunspot number, and planetary magnetic index) to be specified by the user. Departures from the "mean" behavior for a given set of state parameters are not accounted for. This and other limitations of the model are described in Section V of this volume, in which we present our conclusions from this work.

II SIGNAL STATISTICS AND PROPAGATION THEORY

A. Heuristic Description

The transionospheric communication channel may be regarded as a linear filter, the transfer function of which varies temporally and spatially. Fundamentally, the ionosphere behaves as a dispersive, phase-shifting network for all radio waves. The gross carrier phase shift, group delay, and dispersion introduced all are proportional to the integral of electron density along the principal raypath of a communication link. This integral, the "total electron content" (TEC), displays trend-like variations with location on the earth, time of day, season, and the level of solar/geophysical activity. These trends take place on very large spatial scales (hundreds and thousands of kilometers) and long time scales (tens of minutes and hours), and the communication-channel effects associated with TEC are best treated deterministically. Models of TEC behavior and effects (e.g., Klobuchar, 1975) are available for application to the design and operation of communication and navigation systems and of radars.

The present work addresses effects of smaller-scale (tens of meters to tens of kilometers) ionospheric structure on link performance over shorter time scales (fractions of a second to minutes). Unlike the deterministic effects of TEC, the intensity and phase scintillations produced by the small-scale structure are best described in terms of signal statistics. As described in interim reports on this contract (e.g., Fremouw and Rino, 1976), the signal-statistical model developed is complementary to existing TEC models, in terms of time scale and spatial scale and in terms of link effects.

The large-scale structures identified as trends in TEC produce pure phase trends in CW signals, whereas the unambiguous signature of smaller-scale, scintillation-producing structure is well-developed intensity

3

fluctuation, accompanied by phase variations. The slowest intensity scintillations typically are observed to be relatively weak and to be accompanied by relatively strong phase scintillations.

An example of complex-signal scintillation is presented in Figure 1. The data presented are from the DNA Wideband satellite (Fremouw et al.. 1977). Phase (TEC) trends with Fourier periods greater than 10 s have been removed, as have intensity trends (due to changing range to the satellite, etc.). The complex-signal scintillation clearly is dominated by phase variations, but intensity fluctuations also are present on all Fourier frequencies greater than 0.1 Hz, as is demonstrated in Figures 2 and 3.

Figure 2 illustrates the scintillations contained in Figure 1 that have Fourier periods between 2.5 and 10 s, isolated by means of filtering intensity and phase. The weak intensity variations present are correlated with the strong phase variations that dominate the complex-signal scintil-lation in this period range. The correlation is evident in the complex-plane scatter plot at the top of the figure; that is, there is a marked tendency for a phase advance to be accompanied by a weak fade and for a phase retardation to be accompanied by weak signal enhancement. This is the behavior that would be expected in the geometric-optics (near) zone of large, lenslike ionospheric irregularities.

The scintillations with Fourier periods shorter than 2.5 s are illus-trated in Figure 3, which shows that most of the intensity scintillation occurs in this period range, accompanied by relatively weak phase fluctu-ations. The statistical behavior illustrated is consistent with diffrac-tive scatter by smaller-scale irregularities.

The behavior typified by Figures 2 and 3 prompted us to postulate that the complex envelope, E, of a scintillating signal may be character-ized in terms of the following two-component, signal-statistical model (Fremouw and Rino, 1976):

$$E = E_s E_f = (x_s + iy_s) \exp (\chi_f + i\phi_f) \tag{1}$$

4
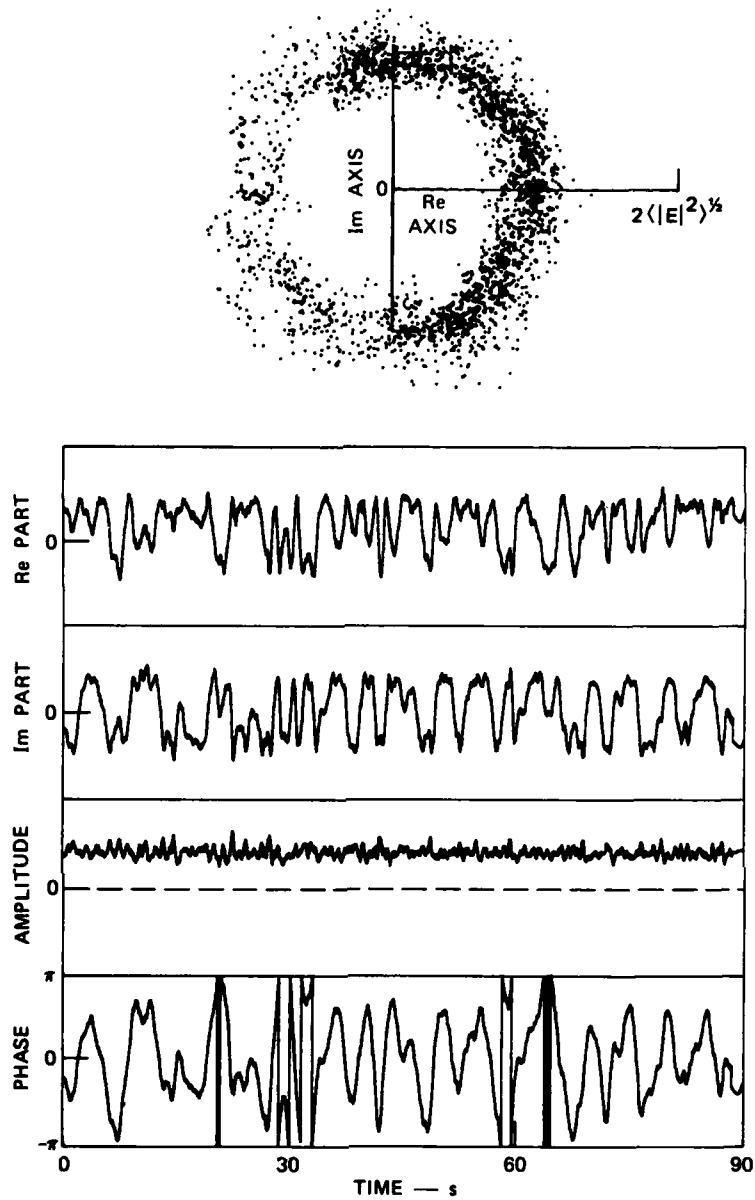
FIGURE 1   THREE REPRESENTATIONS OF VHF (138 MHz) COMPLEX-SIGNAL
            FLUCTUATIONS DURING 90 s OF A SATELLITE PASS OVER STANFORD,
            CALIFORNIA.   Top to bottom: Scatter plot on complex plane; real and
            imaginary parts of complex signal; amplitude and phase of complex signal.
            Intensity and phase scintillation indices are S_4 = 0.28, ana σ_ϕ = 1.58 rad,
            respectively.

5
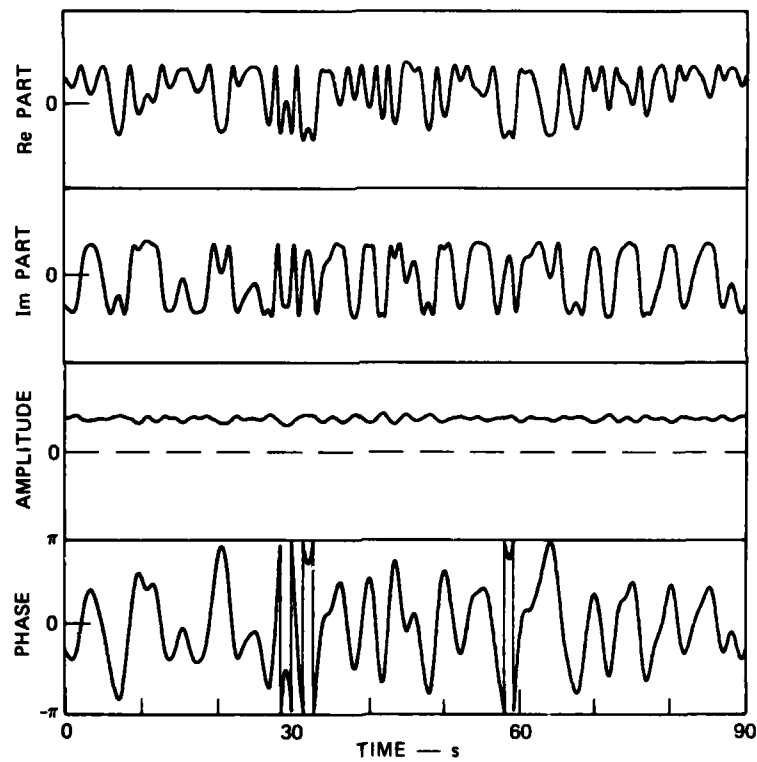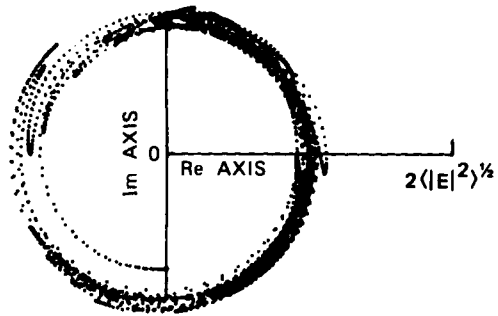
LA-4259-37

FIGURE 2   THE FOCUS COMPONENT (containing intensity and phase fluctuations with Fourier periods shorter than 2.5 s) OF THE COMPLEX-SIGNAL SCINTILLATION PRESENTED IN FIGURE 1

6
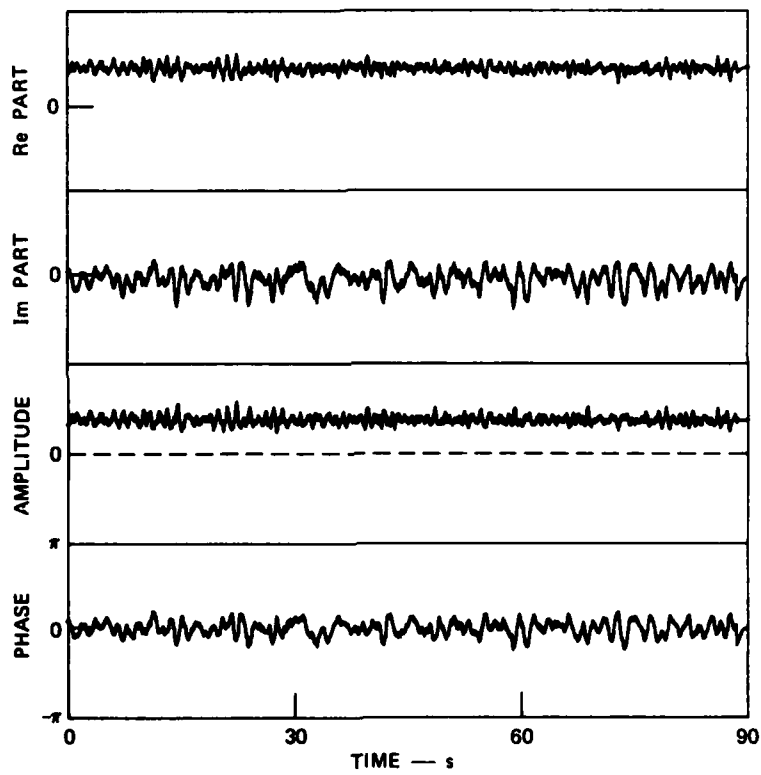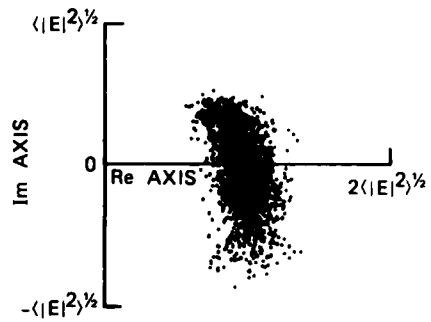
FIGURE 3 THE SCATTER COMPONENT (containing intensity and phase fluctuations with Fourier periods shorter than 2.5 s) OF THE COMPLEX-SIGNAL SCINTILLATION PRESENTED IN FIGURE 1

7

where x_s and y_s are jointly Gaussian variates, as are χ_f and ϕ_f. It is supposed that E_s and E_f are statistically independent. Thus, the first-order statistics of E are totally specified by six (co)variances: σ_x^2, σ_y^2, σ_{xy}, σ_χ^2, σ_ϕ^2, $\sigma_{\chi\phi}$. The "six sigmas" are related to structural parameters of the ionosphere by means of the propagation theory described in Section II-B; the resulting relationships are summarized in Section III-A.

There have long been two intuitive notions about the complex-signal statistics to be expected for a scintillating signal. The first is based on the conceptual model of summation of "randomly" phased contributions from a large number of scattering centers (Ratcliffe, 1956). This notion leads to the suggestion of Rice (1945) statistics or a generalization thereof (Beckman and Spizzichino, 1963), in which the quadrature components of the signal are possibly correlated Gaussian variates with possibly different variances (Rino and Fremouw, 1973; Rino et al., 1976). The second notion is of a radio wave propagating in essentially straight paths along which the phase is randomly increased and decreased in such a way that the output phase is a Gaussian variate (Bramley, 1955). A natural extension of this view is to suppose that the real and imaginary parts of the logarithm of the signal are normal variates.

The two-component model defined above is simply a unification of the foregoing two notions in a way suggested by the first definitive complex-signal scintillation data to become available. The two components are multiplicative because they were isolated experimentally by a process equivalent to a coherent AGC circuit. Heuristically, the components might be expected to be multiplicative because they stem from additive perturbations of the imaginary part of the complex logarithm (i.e., phase). A partial formalizing of the two-component propagation theory is described in Section II-B.

Our propagation calculations employ (1) the phase-screen approach to describing the wave perturbation imposed by ionospheric structure, subject to the Markov approximation, and (2) the parabolic-wave equation for calculating diffraction effects, which is appropriate for all narrow-angle scatter problems. The unique feature of the approach is partitioning

8

of the ionospheric spatial spectrum into two scale-size regimes (of no geophysical significance) to permit efficient computation and to incorporate the empirically derived two-component signal-statistical model. In essence, the computations are divided into one that accounts fully for diffractive scatter by relatively small-scale irregularities and one that employs the ray-optics approximation appropriate for efficient evaluation of focusing and defocusing by larger-scale irregularities.

A heuristic picture of the two-component model might be of a wave encountering a scattering layer, emerging with a scattered and a non-scattered part, and then passing through a region of larger phase-perturbing structure. The phase of both the scattered and nonscattered parts would be spatially modulated by the second region. Statistically, at least, the results would be the same if the positions of the two perturbation processes occurred in the same region. In this heuristic view, one might suppose that only the coherent (nonscattered) part of the scatter component would produce focuses after propagating through the large-scale, phase-perturbing screen. There is some evidence to support this supposition in data from the DNA Wideband satellite, and we have imposed a focusing limit in the model.

B.   Mathematical Development

To develop a mathematical formalism that will allow us to · late the parameters that characterize the first-order signal statistics to the irregularities that ultimately cause the scintillation, we first consider the parabolic-wave equation,

$$\frac{\partial E(\vec{r},z)}{\partial z} = -i \frac{\lambda}{4\pi} \nabla_T^2 E(\vec{r},z) + ir_e \lambda \, \Delta N(\vec{r},z) \, E(\vec{r},z) \quad . \qquad (2)$$

By making the partition

$$\Delta N = \Delta N_s + \Delta N_f \qquad (3)$$

in Eq. (2), where ΔN_s gives rise to the scatter component and ΔN_f gives

9

rise to the focus component, and substituting $E = E_s E_f$ from Eq. (1) into Eq. (2), we obtain the coupled differential equations,

$$\frac{\partial E_s}{\partial \vec{\ell}} = -i \frac{\lambda}{4\pi} \nabla_T^2 E_s + i r_e \lambda \Delta N_s E_s - i \frac{\lambda}{2\pi} \left(\frac{\nabla_T E_f}{E_f} \right) \nabla_T E_s \qquad (4a)$$

and

$$\frac{\partial E_f}{\partial \vec{\ell}} = -i \frac{\lambda}{4\pi} \nabla_T^2 E_f + i r_e \lambda \Delta N_f E_f \qquad . \qquad (4b)$$

The second equation is solved for the log amplitude, χ_f, and phase, ϕ_f, of E_f by using the ray optics approximations

$$\phi_f \cong r_e \lambda \sec \theta \int_0^L \Delta N_f \left(\vec{\rho}_s + \tan \theta \, \hat{a}_{k_T} \, z, z \right) dz \qquad (5)$$

and

$$\frac{\partial \chi_f}{\partial \vec{\ell}} \cong \frac{1}{2k} \nabla_T^2 \phi_f \qquad (6)$$

where

$$\vec{\rho}_s = \vec{\rho} - \tan \theta \, \hat{a}_{k_T} \, z \qquad . \qquad (7)$$

The notation used here is defined in Rino and Fremouw (1977).

From Eqs. (5) and (6) it follows that

$$\left\langle \chi_f \phi_f \right\rangle = \left(\frac{\lambda z \, \sec \theta}{4\pi} \right)^2 \left[a_{11} \frac{\partial^2 R_{\phi_t}}{\partial \Delta \rho_x^2} + 2 \, a_{12} \frac{\partial^2 R_{\phi_f}}{\partial \Delta \rho_x \partial \Delta \rho_y} + a_{22} \frac{\partial^2 R_{\phi_f}}{\partial \Delta \rho_y^2} \right] \qquad (8)$$

and that

10

$$\langle \chi_f \chi_f' \rangle = \frac{\lambda z \sec \theta}{4\pi} \left[a_{11}^2 \frac{\partial^4 R_{\phi_f}}{\partial \Delta \rho_x^4} + 4a_{12} \frac{\partial^4 R_{\phi_f}}{\partial \Delta \rho_x^3 \partial \Delta \rho_y} + \left(4a_{12}^2 + 2a_{11}a_{22} \right) \frac{\partial^4 R_{\phi_f}}{\partial \Delta \rho_x^2 \partial \Delta \rho_y^2} \right.$$
$$\left. + 4a_{12}a_{22} \frac{\partial^4 R_{\phi_f}}{\partial \Delta \rho_x^2 \partial \Delta \rho_y^3} + a_{22}^2 \frac{\partial^4 R_{\phi_f}}{\partial \Delta \rho_y^4} \right] \tag{9}$$

where R_{ϕ_f} is the phase autocorrelation function. The coefficients a_{11} are defined in the companion volume, as is the form of the phase auto-correlation function.

The scatter component is more difficult because the near-zone approxi-mation cannot be made. Moreover, we must also consider the coupling term in Eq. (4a). We assume, however, that the partitioning in Eq. (3) is such that the scale for changes in $\nabla_T E_f / E_f$ (i.e., $\nabla_T \, \ln E_f$) is much larger than the scale for changes in $\nabla_T E_s$. Then Eq. (4b) can be solved as if the $\nabla_T E_f / E_f$ term were constant. In this case, it can be shown that the gradient term makes no contribution to the second-order moments of E_s. If we make the further assumption that E_s is Gaussian, the second-order moments completely specify the statistics of E_s. If follows that the $\nabla_T^2 E_f / E_f$ term has no effect on the statistics of E_s--that is, E_s and E_f are statistically independent.

By this argument, we can neglect the coupling term in Eq. (4a). To then solve Eq. (4a), we use the phase-screen approximation so that

$$E_s \left(\vec{\rho}, z \right) = \iint F \left(\vec{\rho} - \vec{\rho}' \right) \exp \left\{ i \, \phi_s \left(\vec{\rho}' \right) \right\} d\vec{\rho}' \tag{10}$$

where $F(\vec{\rho} - \vec{\rho}')$ is the free-space diffraction kernel for a wavefield scattered through narrow angles. Because E_s is Gaussian, its statistics are completely specified by the second-order coherence functions $R_s = \langle E_s E_s' {}^* \rangle$ and $B_s = \langle E_s E_s' \rangle$.

When R_s is computed using Eq. (10), the diffraction kernel becomes a delta function so that R_s does not vary with z. Thus, a simple analytic

11

formula that is given in Section 2 of the Appendix of the companion volume (Rino et al., 1977), can be used. For B_s a formula very similar to Eq. (10) results, which must be evaluated numerically. The details are described in the companion volume.

To summarize, as long as E_s is Gaussian and the scale for changes in $\nabla_T \ln E_f$ is very large compared to the scale for changes in $\nabla_T E_s$, we can relate the multiplicative scatter and focus components to disjoint and therefore independent spectral scale size regimes of the contributing irregularities. From these relations we can calculate the signal moments that describe the field as a function of parameters that characterize the spectrum of the ionospheric irregularities. This constitutes the formal basis of all the mathematical computations used in the code.

12

III SCINTILLATION MORPHOLOGY

A. Controlling Parameters

As will be outlined in Section IV, two computer codes have been de-
veloped under this contract. The primary scintillation calculations are
performed in the more elaborate of the two codes, IONSCNT. There are
two operational modes in IONSCNT, one to provide first-order signal-
statistical parameters and one to provide second-order quantities. The
ultimate outputs of the first-order mode are the six sigmas that charac-
terize the two-component scintillation model and the scintillation indices
for phase, ϕ, and intensity, I, which are defined respectively as follows:

$$\sigma_{\phi} = \left[\langle \phi^2 \rangle - \langle \phi \rangle^2 \right]^{\frac{1}{2}} \tag{11}$$

$$S_4 = \frac{\left[\langle I^2 \rangle - \langle I \rangle^2 \right]^{\frac{1}{2}}}{\langle I \rangle} \quad . \tag{12}$$

According to the two-component model, the phase and intensity scintil-
lation indices for the composite signal are given in terms of those for
the scatter and focus components as:

$$\sigma_{\phi}^2 = \sigma_{\phi_s}^2 + \sigma_{\phi_f}^2 \tag{13}$$

and

$$S_4^2 = \left(S_{4_s}^2 + 1 \right) \left(S_{4_f}^2 + 1 \right) - 1 \quad . \tag{14}$$

The component indices are obtained as follows. The most complicated
is the phase scintillation index for the scatter component. It is ob-
tained by performing the following two integrations:

13

$$\langle \phi_s \rangle = \int_o^{2\pi} \phi_s \ P_h \left(\phi_s; \ \sigma_{x_s}, \ \sigma_{y_s}, \ \sigma_{x_s y_s} \right) d\phi_s \qquad (15)$$

and

$$\phi^2 = \int_o^{2\pi} \phi_s^2 \ P_H \left(\phi_s; \ \sigma_{x_s}, \ \sigma_{y_s}, \ \sigma_{x_s y_s} \right) d\phi_s \qquad (16)$$

over P_H, the Hatfield phase distribution for a signal with complex Gaussian statistics. The Hatfield distribution (Hatfield and Rino, 1975) is specified by

$$\sigma_{x_s}^2 = \frac{1}{2} \left[R_{os} - \text{Re} \left\{ B_{os} \right\} \right] \qquad (17)$$

$$\sigma_{y_s}^2 = \frac{1}{2} \left[R_{os} + \text{Re} \left\{ B_{os} \right\} \right] \qquad (18)$$

$$\sigma_{x_s y_s}^2 = \frac{1}{2} \text{Im} \left\{ B_{os} \right\} \qquad (19)$$

where

$$R_{os} = 1 - e^{-\sigma_s^2 L} \qquad (20)$$

where σ_s^2 is a scattering coefficient per unit depth in a layer of thickness L [see Eq. (31)], and B_{os} is obtained from numerical evaluation of the diffraction integrals by a procedure described in the companion volume (Rino et al., 1977). The quantities above are also used to calculate the intensity scintillation index for the scatter component, as follows:

$$S_{4s}^2 = 4\sigma_{x_x}^2 \left(1 - R_{os} \right) + \left| B_{os} \right|^2 \quad . \qquad (21)$$

The phase and intensity scintillation indices for the focus component are calculated, respectively, as

$$\sigma_{\phi f}^2 = \sigma_f^2 \ L - \sigma_{\chi_f}^2 \qquad (22)$$

14

and

$$S_{4f} = e^{\sigma^2_{\chi_f}} - 1 \qquad (22)$$

where $\sigma^2_f L$ is the variance of phase perturbation imposed by a layer of thickness L [see Eq. (30)], and $\sigma^2_{\chi_f}$ is obtained from numerical evaluation of differential equations derived from the geometric-optics approximation of the parabolic wave equation, as described in Section II-B; the same approximation is used to calculate $\sigma_{\chi_f \phi_f}$.

The propagation equations that govern B_{os}, $\sigma^2_{\chi_f}$, and $\sigma_{\chi_f \phi_f}$ depend upon the observing geometry relative to a horizontally stratified ionospheric layer and to a geomagnetic field model and upon several parameters that characterize the size and shape of ionospheric irregularities. As described in the companion volume, the three-dimensional spatial power spectrum employed to describe the irregularities has a power-law form with a spectral index of minus four, corresponding to an in-situ (one dimensional) spectrum of κ^{-2}. Provision is made for anisotropy in two dimensions, one along the magnetic field and one perpendicular to the field. The spectrum over which the variance of ionospheric electron density, $\langle (\Delta N)^2 \rangle$, is modeled is limited by an outer-scale parameter, α_f, and the spectrum is divided into two components by means of an inner-scale cutoff for the focus component, β_f, and an outer-scale parameter for the scatter component, α_s.

B. Behavior of Axial Ratios, Scale Sizes, and Height

The axial ratios, a (along the field) and b (perpendicular to the geomagnetic meridian plane) were set to reproduce known geometrical characteristics of scintillation. Interferometer observations have shown that scintillation-producing irregularities are highly elongated along the magnetic field near the geomagnetic equator (e.g., Koster et al., 1966). Recent studies by Rino (1977) indicate that high-latitude irregularities are somewhat elongated perpendicular to the geomagnetic meridian as well as along the magnetic field (i.e., that they are sheet-like along L-shells rather than axially symmetric along the field).

15

To include the foregoing experimental characteristics, the axial ratios a and b have been modeled as functions of geomagnetic latitude, λ_m, as follows:

$$a = 30 - 10 \left(1 + \text{erf } \frac{\lambda_m - 20°}{3°} \right) \tag{24}$$

and

$$b = 1 + 2.5 \left(1 + \text{erf } \frac{\lambda_m - \lambda_b}{3°} \right) \tag{25}$$

where λ_b demarks the geomagnetic latitude of the scintillation boundary between the midlatitude ionosphere and the subauroral ionosphere. Equation (24) provides an along-field axial ratio of 30 near the geomagnetic equator, switching to 10 fairly abruptly at a geomagnetic latitude of 20°. Equation (25) describes axial symmetry at latitudes equatorward of the scintillation boundary. Poleward of the boundary there is an additional elongation in the geomagnetic east-west direction, with a ratio of 6:1 (b = 6) relative to the remaining cross-field dimension.

The three scale parameters α_f, β_f, and α_s were established by iterative testing against signal-statistical samples obtained from passes of the DNA Wideband satellite. The most satisfactory fits were found to be different at different latitudes. (No data were available from the polar caps.) Variation of the scale-size parameters with geomagnetic latitude, λ_m, has been modeled as follows:

$$\alpha_f = 900 + 850 \left(1 + \text{erf } \frac{\lambda_m - 20°}{3°} \right) \text{meters} \tag{26}$$

$$\beta_f = \alpha_f / 2.5 \tag{27}$$

and

$$\alpha_s = \alpha_f / 4 \quad . \tag{28}$$

16

Equation (26) provides an outer scale (transverse to the magnetic field) of just under 1 km (i.e., approximately equal to the Fresnel-zone radius for VHF waves in the F layer) near the geomagnetic equator and of about 2.6 km poleward of 20° geomagnetic latitude. It is to be noted that the actual outer scale of ionospheric irregularities probably is considerably greater than one or a few kilometers; the present model accounts only for irregularities that produce scintillation, defined in terms of intensity fluctuation. Equations (27) and (28) are used to maintain effective continuity between the focus and scatter components of the spatial spectrum employed, while also safeguarding validity of the ray-optics approximation used for calculating propagation of the focus component of the perturbed wave.

The reason for employing a smaller outer scale in the equatorial region than elsewhere is that we have consistently observed with the DNA Wideband satellite that the ratio of S_4 to σ_ϕ is larger (unless, of course, S_4 is near its limiting value of approximately unity) in the equatorial region than elsewhere, for data processed in an identical fashion. In terms of the phase-screen model, this observed fact means that a given level of phase perturbation (within the spatial spectrum admitted by 10-s detrending) results in stronger propagation effects (focusing and diffraction) near the equator than at higher latitudes. Employing a smaller outer scale for a given level of $\langle (\Delta N)^2 \rangle$ is one way of accounting for such behavior. A systematic decrease in the spectral index with decreasing latitude also could account for this effect. A variable spectral index, however, greatly complicates the computer code. Thus, we have not incorporated this option.

A greater propagation distance (i.e., employing a greater scattering-layer height) also increases the level of intensity scintillation. There is evidence from backscatter observations (Woodman and La Hoz, 1976), for development of fine structure from the bottomside to the topside of the equatorial ionosphere. We have incorporated a simple latitude dependence of scattering-layer height in the model, as follows:

$$H = 500 - 75 \left(1 + \text{erf} \, \frac{\lambda_m - 20°}{3°}\right) \text{km} \qquad (29)$$

which places the center of the layer at 350 km at geomagnetic latitudes greater than about 20° and at 500 km near the magnetic equator.

C. Behavior of Scattering Strength

Once geometric and signal-statistical behavior is modeled by choice of axial ratios, scale sizes, and height, the worldwide morphological behavior of scattering strength is the dominant consideration for scintillation modeling. The total disturbance imposed on the wave consists of the wavefront perturbation imparted by both the focus and scatter portions of the spatial spectrum, whose integral is $\langle(\Delta N)^2\rangle$. For the focus component, the variance of the phase perturbation imposed by a layer of thickness L is given by

$$\sigma_f^2 L = r_e^2 \, \lambda^2 \, \frac{ab\sqrt{\beta_f} \langle(\Delta N)_f^2\rangle}{G \cos \theta} \, L \, \sec \, \theta \left[\sqrt{2\pi} \, \frac{K_1\left(2\beta_f/\alpha_f\right)}{K_{\frac{1}{2}}\left(2\beta_f/\alpha_f\right)}\right] . \qquad (30)$$

The corresponding quantity for the scatter component is

$$\sigma_s^2 L = r_e^2 \, \lambda^2 \, \frac{ab\alpha_s \langle(\Delta N)_s^2\rangle}{G \cos \theta} \, L \, \sec \, \theta \qquad (31)$$

where θ is the incidence angle on the layer, G depends on details of the scattering geometry through the anisotropy of the irregularities, r_e is the classical electron radius, λ is the radio wavelength, and the K's denote the modified Bessel function.

All the geophysical parameters in Eqs. (30) and (31) were discussed in Section III-B, except L and $\langle(\Delta N)^2\rangle = \langle(\Delta N)_s^2\rangle + \langle(\Delta N)_f^2\rangle$. In conjunction with the latitudinal dependence of layer height, the layer thickness also was modeled as a simple function of geomagnetic latitude, as follows:

18

$$L = 200 - 50 \left(1 + \mathrm{erf}\ \frac{\lambda_m - 20°}{3°} \right) \mathrm{km} \qquad . \tag{32}$$

With α_f and α_s set, the relative amount of perturbation assigned to the focus and scatter components is that required for their respective spectra to be asymptotically continuous. The condition is

$$\left\langle (\Delta N)_f^2 \right\rangle = \frac{\alpha_f}{\alpha_s} \left\langle (\Delta N)_s^2 \right\rangle \qquad . \tag{33}$$

Finally, observed morphological characteristics of intensity and phase scintillation were invoked to write the following mean, morphological description of $\left\langle (\Delta N)^2 \right\rangle$:

$$\left\langle (\Delta N)_s^2 \right\rangle^{\frac{1}{2}} = \Delta N_m \left(\lambda_m, T \right) + \Delta N_h \left(\lambda_m, T, K_p \right) + \Delta N_a \left(\lambda_m, T, K_p \right)$$

$$+ \Delta N_e \left(\lambda_m, \lambda_g, T, D, R \right) \qquad . \tag{34}$$

The first two terms and the last term on the right of Eq. (34) account for behavior at, respectively, middle, high, and equatorial latitudes, as functions of geomagnetic latitude, λ_m, geographic latitude, λ_g, local time of day in hours, T, day of the year, D, mean sunspot number, R, and the planetary magnetic activity index, K_p. The third term in Eq. (34) accounts for scintillation associated with the auroral oval.

The midlatitude term, centered at a geomagnetic latitude of 32.5°, contains only a simple diurnal variation, as follows:

$$\Delta N_m = 1.3 \times 10^9 \left(1 + 0.33 \cos \frac{\pi T}{12} \right) \exp \left[\frac{\left(\lambda_m - 32.5° \right)^2}{(15°)^2} \right] \qquad . \tag{35}$$

The high-latitude term,

$$\Delta N_h = 3 \times 10^9 \left(1 + \mathrm{erf}\ \frac{\lambda_m - \lambda_b}{\lambda_h} \right) \mathrm{el/m}^3, \tag{36}$$

dominates poleward of the scintillation boundary, the geomagnetic latitude and width of which vary with magnetic activity and time of day as follows:

19

$$\lambda_b = 68.5 - 1.8 \ K_p - \left(5 + 0.5 \ K_p\right) \cos \frac{\pi T}{12} \ \text{deg} \qquad (37)$$

$$\lambda_h = 5 + 0.2 \ \lambda_b \ \text{deg} \qquad . \qquad (38)$$

Superimposed on the high-latitude term is the following auroral-oval term:

$$\Delta N_a = 3.2 \times 10^8 \ K_p \ \exp \left[- \frac{\left(\lambda_m - \lambda_a\right)^2}{\left(1.1 \ K_p\right)^2} \right] \ \text{el/m}^3 \qquad (39)$$

where

$$\lambda_a = 74 - 1.8 \ K_p \ \cos \frac{\pi T}{12} \ \text{deg} \qquad . \qquad (40)$$

The most complicated term in the morphological model is the following one describing behavior near the geomagnetic equator:

$$\Delta N_e = 2.3 \times 10^9 \ (1 + 0.04R) \left\{ \exp \left[- \frac{\left(\lambda_m - 10°\right)^2}{\left(10°\right)^2} \right] + \exp \left[- \frac{\left(\lambda_m + 10°\right)^2}{\left(10°\right)^2} \right] \right\}$$

$$\left\{ 1 - 0.4 \left[\cos \frac{\pi(D + 10)}{91} + \frac{\lambda_g}{15°} \cos \frac{\pi(D + 10)}{182} \right] \right\}$$

$$\left\{ \exp \left[- \frac{(T + 1.5)^2}{(6)^2} \right] + \exp \left[- \frac{(T - 22.5)^2}{T_R^2} \right] \right\} \text{el/m}^3 \qquad (41)$$

where

$$T_R = \frac{3}{6} \ \text{if} \ T \lessgtr 22.5 \qquad .$$

Equation (41) describes a region of disturbance that peaks some 10° on each side of the geomagnetic equator. This somewhat speculative morphological behavior has been invoked to account for a very persistent feature of scintillation observed at Ancon, Peru and Kwajalein, Marshall Islands

20

(both within a few degrees of the magnetic equator) on signals from the DNA Wideband satellite. The persistent behavior is an increase in scintillation near the ends of satellite passes that is stronger than we have been able to account for on the basis of any purely geometrical feature of the model.

Equation (41) also includes a linear increase of scintillation activity with increasing sunspot number, and a diurnal peak somewhat before local midnight, with activity increasing rather rapidly after F-layer sunset and decaying more slowly after the peak. The seasonal variation includes equinoctial peaking but with a "filling in" of activity in the local summer season (i.e., centered on the December solstice in the geographic southern hemisphere and on the June solstice in the geographic northern hemisphere). This somewhat complicated behavior is consistent with differences in seasonal patterns observed at Kwajalein and at Ancon and reproduces reasonably well the equinoctial peaking observed by Koster (1966) and Koster et al. (1966) for observations at a station near the geographic equator in Africa; it is untested at other locations, however.

IV COMPUTER CODES

Two user codes have been developed under this contract: IONSCNT for calculating first-order and second-order signal-statistical moments, including scintillation indices for intensity and for phase and several correlation functions; and DIST for calculating first-order, probability-density functions (PDFS) for intensity and phase and the corresponding cumulative distribution functions (CDFS).

Figure 4 shows a simplified, overall flow diagram for IONSCNT. The user inputs a set of selected ionospheric state parameters plus a description of his intended operational geometry. The code then calculates the appropriate ionospheric structure parameters from the morphological model contained in subroutines RMSDN and MDLPRM. The quantities relevant to the scatter and focus components are passed to routines for calculating diffraction and geometric-optics propagation effects, respectively.

The outputs from IONSCNT always include the intensity and phase scintillation indices, S_4 and σ_ϕ, and the six sigmas that describe the two-component, first-order, signal-statistical model. If the user has selected operating Mode II, second-order statistical counterparts are put out as well, including the temporal autocorrelation functions of intensity and phase, analogous information on the spatial autocorrelation function, and (if requested) the correlation coefficient for intensity fluctuations on two user-selected frequencies.

The temporal autocorrelation functions are computed from the calculated spatial autocorrelation function, using a velocity that accounts both for line-of-sight motion through the F layer and an assumed drift of otherwise unchanging ionospheric structure. The drift velocity is eastward at a speed given by the following geomagnetic-latitude-dependent model:

$$V_d = 50 - 15 \left(1 + \text{erf}\ \frac{\lambda_m - 20°}{3°}\right) + 40 \left(1 + K_p\right)\left(1 + \frac{\lambda_m - \lambda_b}{3°}\right) \quad (42)$$

which yields 50 m/s in the equatorial zone, 20 m/s at middle latitudes, and upwards of 100 m/s poleward of the subauroral scintillation boundaries, depending on the level of geomagnetic disturbance.

An example of the Mode-I output of IONSCNT is presented in Figure 5. The increase in scintillation early in the second half of the pass arises from a combination of (1) geometric enhancement by sheet-like irregularities
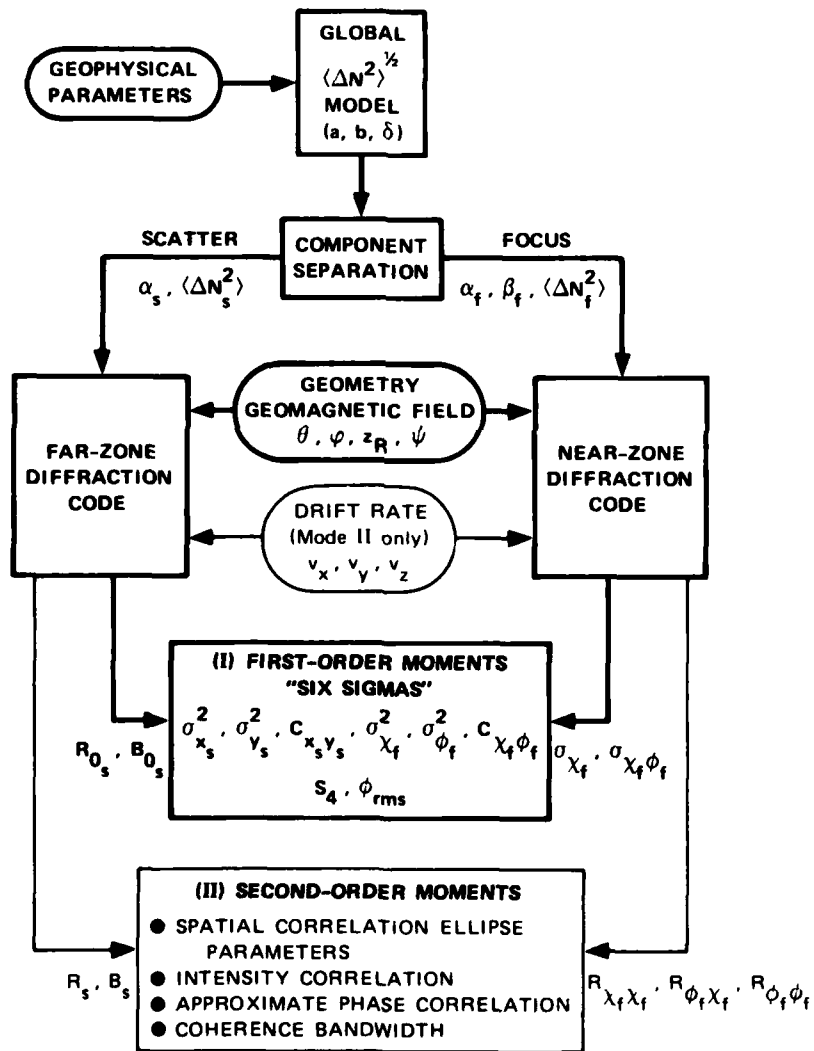
LA-4259-29

FIGURE 4   SIMPLIFIED FLOW DIAGRAM FOR THE MAIN
COMPUTER CODE, IONSCNT

24

F-LAYER PRODUCED VHF-UHF SCINTILLATION

CALCULATED FROM A MODEL DEVELOPED BY STANFORD RESEARCH INSTITUTE,
MENLO PARK, CALIFORNIA.

AURORAL

INPUT CONDITIONS USED FOR THIS CALCULATION WERE :

FREQUENCY= 137.68 MHZ   SUNSPOT NO.= 50.   DAY 150, OUT OF 365   KP INDEX = 5.00   TIME= 2.30 LMT AT RECEIVER

RECEIVER COORDINATES LAT= 65.13 DEG   LONG=-147.49 DEG   ALT= .195 KM
TRANSMITTER COORDINATES LAT= 79.60 DEG   LONG= -80.30 DEG   ALT= 1000.000 KM   FOR FIRST ORBIT POINT

(FOR THIS RUN) THE CHANGING PARAMETERS WERE: TRANSMITTER LATITUDE AND LONGITUDE ALONG ORBIT)

	T-LAT	T-LONG	PSIWP	SGX2	SGY2	CRXY	SGLA2	SGPH2	CRLAPH	S4	PRMS
1	79.393	-80.332	76.364	.07756	.31279	-.00032	.00001	8.59309	-.00323	.63904	171.489
2	80.042	-92.056	75.875	.07066	.39171	-.00019	.00001	8.08937	-.00286	.60789	166.357
3	80.269	-104.801	74.875	.06357	.28934	-.00404	.00000	7.55834	-.00251	.58323	160.803
4	79.989	-117.478	73.317	.05706	.27697	-.00398	.00000	7.05047	-.00222	.55959	155.399
5	79.294	-129.035	71.158	.05191	.26636	-.00391	.00000	6.65264	-.00199	.53150	150.865
6	78.263	-138.900	68.366	.04490	.25972	-.00343	.00000	6.40872	-.00186	.52441	149.079
7	76.919	-147.012	64.967	.04911	.25992	-.00412	.00000	6.41886	-.00187	.52511	148.156
8	75.398	-153.593	61.094	.05458	.27097	-.00467	.00000	6.83920	-.00214	.54787	152.963
9	73.735	-158.937	57.024	.07024	.24605	-.00593	.00001	7.99800	-.00301	.60692	165.425
10	71.968	-163.316	53.303	.10933	.35111	-.00656	.00002	10.71388	-.00580	.71192	191.679
11	70.126	-166.951	50.524	.20584	.44735	-.01260	.00011	17.41488	-.01740	.86901	245.460
12	68.228	-170.010	49.081	.36895	.48633	-.01151	.00067	33.32540	-.06531	.98650	339.896
13	66.287	-172.620	48.924	.36639	.48413	-.01123	.00065	33.00260	-.05655	.98081	338.262
14	64.313	-174.875	47.656	.27195	.45839	-.01226	.00015	22.75736	-.02301	.62911	281.021
15	62.313	-176.849	50.801	.21471	.43300	-.01184	.00006	18.11635	-.01284	.67790	250.426
16	60.292	-178.595	51.592	.18077	.41259	-.01140	.00003	15.02494	-.00919	.83701	232.278
17	58.254	179.845	52.997	.15357	.39198	-.01140	.00002	13.69480	-.00748	.79041	217.190
18	56.202	178.438	53.690	.12549	.36547	-.01170	.00002	11.72445	-.00641	.74481	200.669
19	54.140	177.158	54.009	.09571	.32973	-.01197	.00002	9.62259	-.00556	.67958	181.572
20	52.068	175.985	53.928	.06928	.28620	-.01211	.00002	7.69016	-.00491	.59171	161.260
21	49.988	174.903	53.436	.04777	.24080	-.01276	.00002	5.91220	-.00486	.50719	142.242

* INDICATES ACCURACY OF VALUE MAY BE QUESTIONABLE DUE TO POOR INTEGRATION CONVERGENCE

LA-4259-40

FIGURE 5   EXAMPLE OF MODE-I OUTPUT FOR IONSCNT. The intensity and phase scintillation indices (S4 and PRMS, respectively) appear in the rightmost two columns.

as the line of sight grazes the L-shell through the station, and (2) a contribution from the auroral term in Eq. (34). Graphs of S_4 and ϕ_{rms} for a representative pass of the Wideband satellite observed at Poker Flat, Alaska under the specified conditions are shown in Figure 6 for comparison.
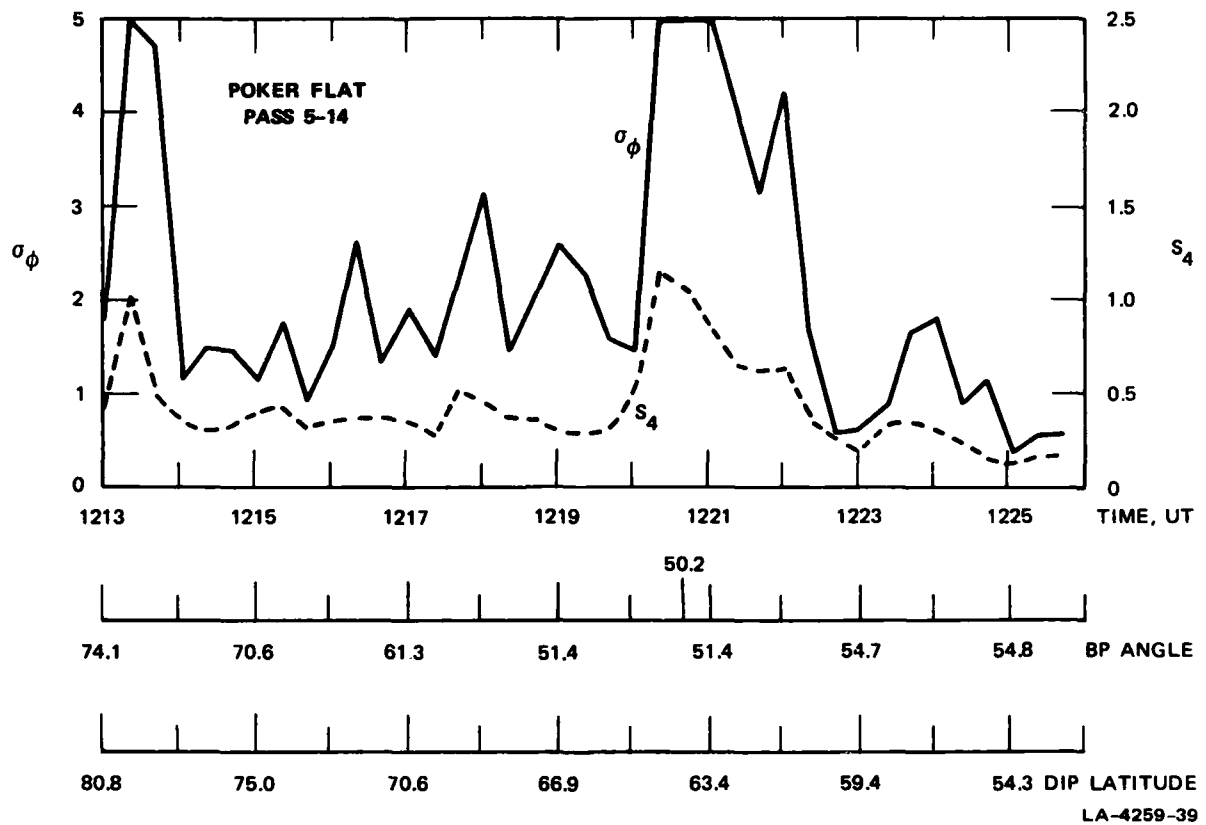

FIGURE 6 STANDARD SUMMARY DISPLAY OF VHF (138 MHz) INTENSITY AND PHASE SCINTILLATION INDICES (S_4 and σ_ϕ, respectively) OBSERVED IN ALASKA ON A PARTICULAR SATELLITE PASS UNDER CONDITIONS APPROXIMATED BY THE INPUT CONDITIONS FOR THE CALCULATION ILLUSTRATED IN FIGURE 5

Note that the pass illustrated was one of those used in iterative testing of the model; it was chosen as one representative of scintillation in Alaska under the specified conditions (including moderate magnetic activity). A range of scintillation behavior presumably would be observed for the same set of specified state parameters, and the model does not account for such variations.

26

In addition to the scintillation indices, the output illustrated in Figure 5 gives relatively subtle signal-statistical information, in the form of the six sigmas (four variances and two covariances) that characterize the two first-order, signal-statistical components. They appear in the six columns following the transmitter latitude and longitude and the angle (PSIBP) between the line of sight and the geomagnetic field. Taking point 8 in Figure 5 as an example, we have $\sigma^2_{x_s} = 0.055$, $\sigma^2_{y_s} = 0.271$, $\sigma_{x_s y_s} = -0.005$, $\sigma^2_{\chi_f} = 0.000$, $\sigma^2_{\phi_f} = 6.839$, $\sigma_{\chi_f \phi_f} = -0.002$.

By comparison, the corresponding values for a 30-s data segment (starting at 0217:35) recorded during a geometrically similar portion of the satellite pass illustrated in Figure 6 are 0.06, 0.27, -0.02; 0.01, 4.40, and -0.07. Similarities between the calculated and observed values suggest that the existing model would be useful for calculating the joint pdf of intensity and phase, if the joint statistics should be of interest for, say, optimal system design. Such a capability has not been incorporated in the present computer programs but could be added to the DIST code.

The DIST code now available permits calculation of distributions for amplitude (square root of intensity) and phase, separately. Examples are presented in Figure 7, using the six sigmas from point 8 of Figure 5 as inputs to DIST. As is described fully in the companion volume on the codes (Rino et al., 1977), the method of using DIST is to input the results of an IONSCNT calculation.

Figure 8 illustrates second-order outputs from IONSCNT, again using point 8 from Figure 5; the format is fully described in the companion volume. The information provided can be used to characterize the spatial structure of the field as well as the temporal structure of intensity and phase.

Figures 9 through 14 are included to provide further information on the morphological behavior (and frequency dependence) of scintillation as characterized by IONSCNT. The reader will note that the code returns values of S_4 slightly larger than unity, which is the value corresponding to Rayleigh statistics, under extreme conditions. The two-component,
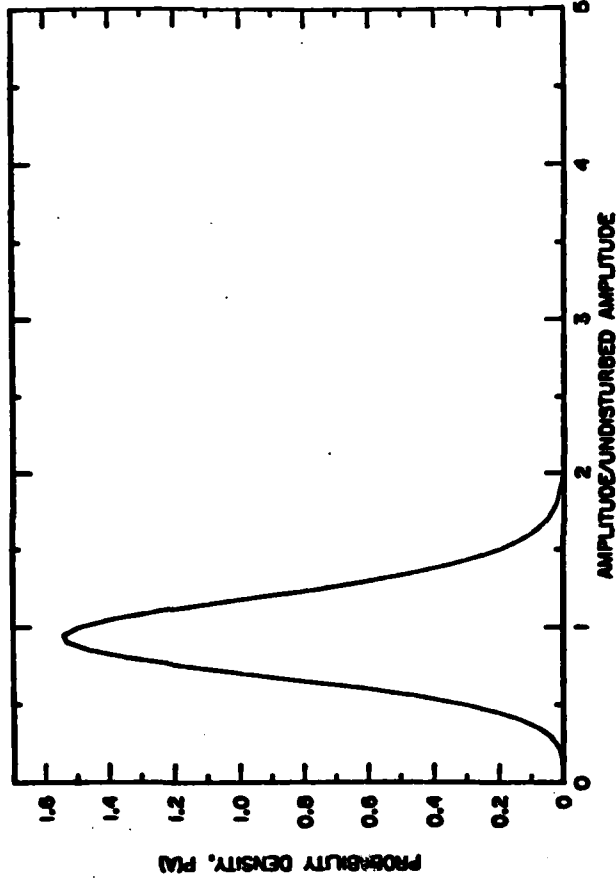
27

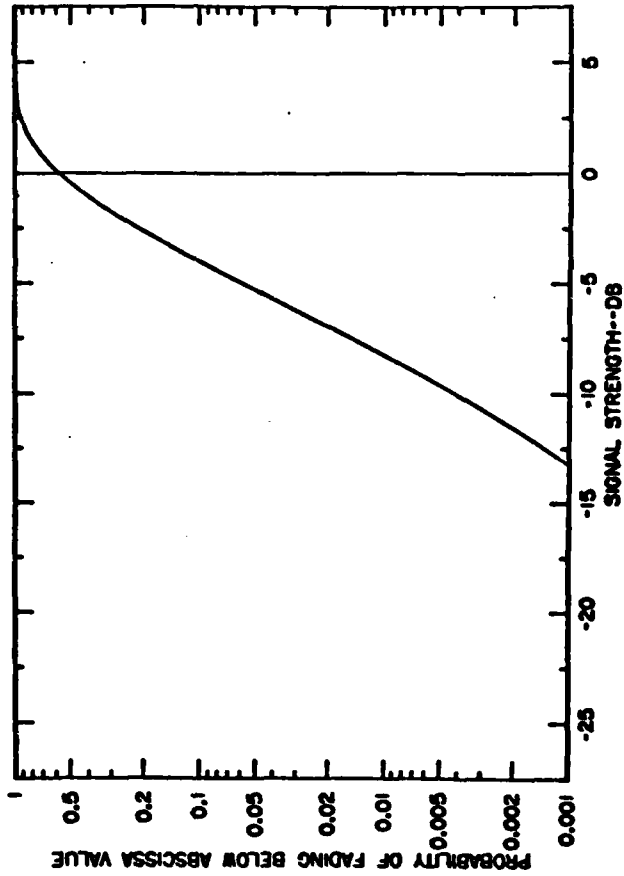(a) PROBABILITY DENSITY FUNCTION FOR AMPLITUDE

FIGURE 7   EXAMPLE OF OUTPUTS FROM DIST CODE, USING IONSCNT RESULTS FROM POINT 8 IN FIGURE 5 AS INPUTS.

LA-4259-41

CUMULATIVE PROBABILITY, CPF, VS. SIGNAL STRENGTH IN DB RELATIVE TO UNDISTURBED LEVEL

SGX2= .055 SGY2= .27 CRXY= .005 SGLA2= .000 SGPH2= 6.84 CRLAPH= .00

DB	CPF	DB	CPF	DB	CPF	DB	CPF	DB	CPF	DB	CPF	DB	CPF
-26.02	.000	-20.00	.000	-16.48	.000	-13.98	.006	-12.04	.001	-10.46	.002	-9.12	.003
-6.94	.020	-6.02	.033	-5.19	.052	-4.44	.078	-3.74	.113	-3.10	.157	-2.50	.211
-1.41	.344	-.92	.419	-.45	.496	.00	.573	.63	.645	1.21	.711	1.58	.770
1.96	.862	2.28	.896	2.61	.923	2.92	.943	3.23	.959	3.52	.970	3.81	.979
4.35	.989	4.61	.992	4.86	.995	5.11	.996	5.34	.997	5.58	.998	5.80	.998
6.24	.999	6.44	.999	6.65	.999	6.85	.999	7.06	.999	7.23	.999	6.02	.999

(b) CUMULATIVE PROBABILITY FUNCTION FOR AMPLITUDE

SGX2= .055 SGY2= .27 CRXY= .005 SGLA2= .000 SGPH2= 6.84 CRLAPH= .00

FIGURE 7   (Continued)

PROBABILITY DENSITY, P(PHI), VS. PHASE ANGLE IN RADIANS

SGX2= .055 SGY2= .27 CRXY= -.005 SGLA2= .000 SGPH2= 6.84 CRLAPH= -.00

PHI	P(PHI)	PHI	P(PHI)	PHI	P(PHI)	PHI	P(PHI)	PHI	P(PHI)	PHI	P(PHI)	PHI	P(PHI)	PHI	P(PHI)
-5.00	.0258	-4.90	.0277	-4.80	.0296	-4.70	.0316	-4.60	.0338	-4.50	.0360	-4.40	.0383	-4.30	.0408
-4.20	.0433	-4.10	.0459	-4.00	.0485	-3.90	.0513	-3.80	.0542	-3.70	.0571	-3.60	.0601	-3.50	.0632
-3.40	.0663	-3.30	.0695	-3.20	.0727	-3.10	.0760	-3.00	.0794	-2.90	.0827	-2.80	.0861	-2.70	.0895
-2.60	.0929	-2.50	.0963	-2.40	.0996	-2.30	.1030	-2.20	.1063	-2.10	.1095	-2.00	.1127	-1.90	.1159
-1.80	.1189	-1.70	.1219	-1.60	.1247	-1.50	.1275	-1.40	.1301	-1.30	.1326	-1.20	.1350	-1.10	.1372
-1.00	.1392	-.90	.1411	-.80	.1428	-.70	.1443	-.60	.1456	-.50	.1468	-.40	.1477	-.30	.1484
-.20	.1490	-.10	.1493	-.00	.1494	.10	.1493	.20	.1490	.30	.1485	.40	.1478	.50	.1468
.60	.1457	.70	.1444	.80	.1429	.90	.1412	1.00	.1394	1.10	.1373	1.20	.1351	1.30	.1328
1.40	.1303	1.50	.1277	1.60	.1250	1.70	.1221	1.80	.1192	1.90	.1161	2.00	.1130	2.10	.1058
2.20	.1065	2.30	.1032	2.40	.0999	2.50	.0965	2.60	.0931	2.70	.0897	2.80	.0863	2.90	.0830
3.00	.0794	3.10	.0763	3.20	.0730	3.30	.0697	3.40	.0665	3.50	.0634	3.60	.0603	3.70	.0573
3.80	.0544	3.90	.0515	4.00	.0488	4.10	.0461	4.20	.0435	4.30	.0409	4.40	.0388	4.50	.0362
4.60	.0360	4.70	.0318	4.80	.0298	4.90	.0278	5.00	.0259						
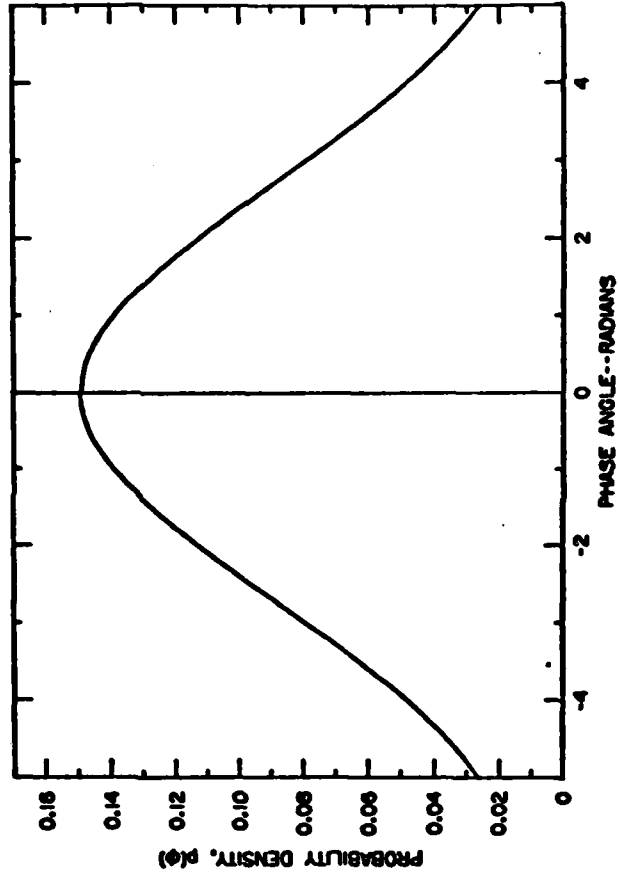
SGX2= .055 SGY2= .27 CRXY= -.005 SGLA2= .000 SGPH2= 6.84 CRLAPH= -.00

(c) PROBABILITY DENSITY FUNCTION FOR PHASE

FIGURE 7   (Concluded)
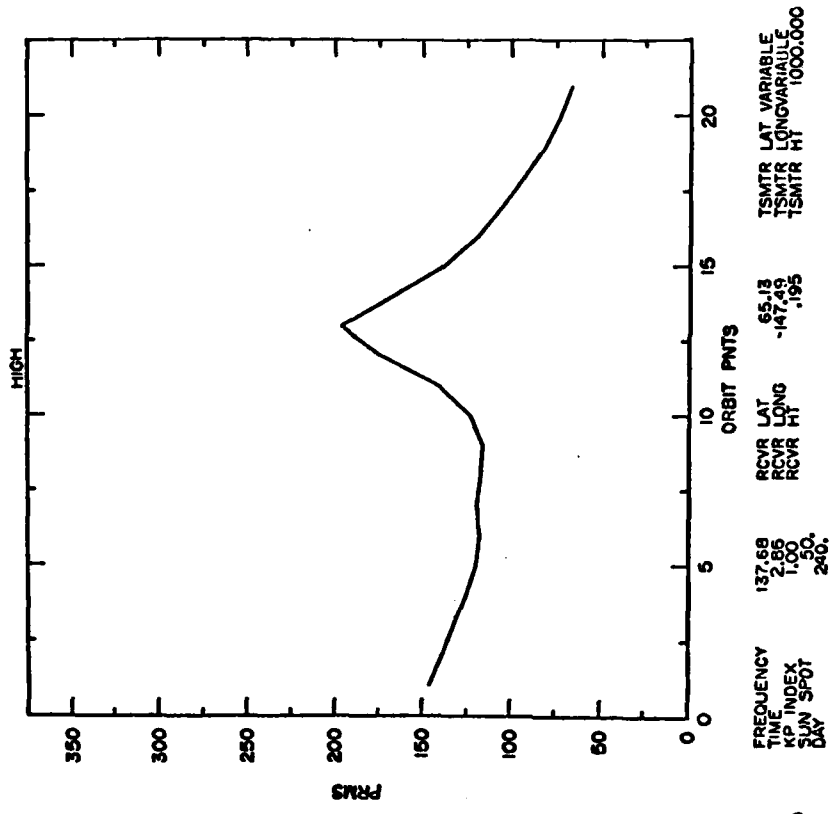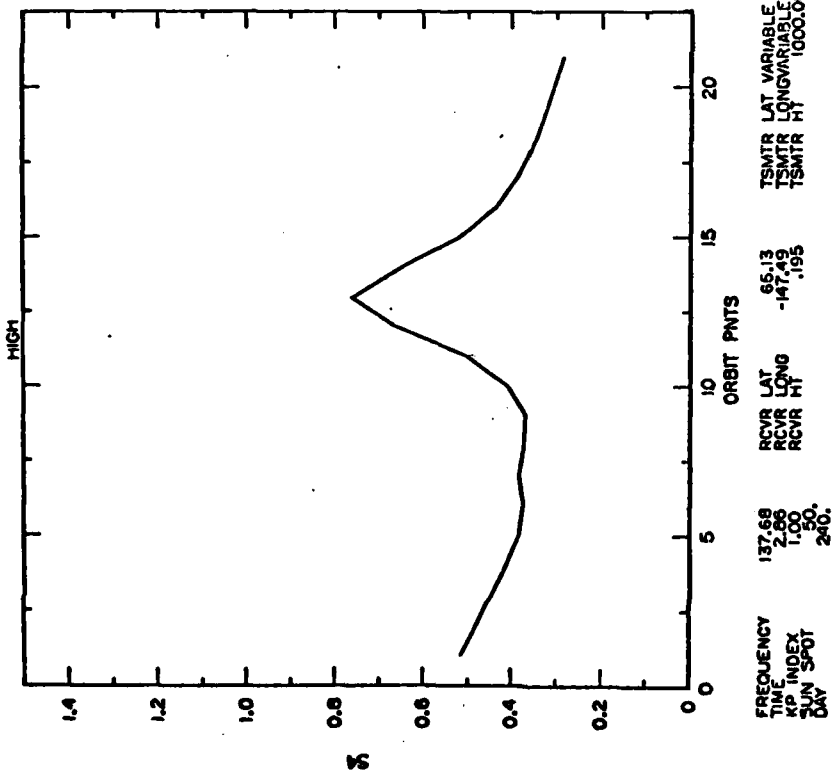
LA-4259-43

30

SECOND-ORDER OUTPUT FOR POINT 8

DIFFRACTION PATTERN
AXIAL RATIO= 3.53
AZ. OF MINOR AXIS= -6.17

SCAN
VEFF= 583.93 M/SEC
AZ. OF SCAN= 28.55

| LAG	LAG	PHASE AUTOCORRELATION FUNCTION			INTENSITY AUTOCORRELATION FUNCTION		
SEC	M	SCATTER	FOCUS	COMPOSITE	SCATTER	FOCUS	COMPOSITE
0.00	0.00	1.00000	1.00000	1.00000	1.00000	1.00000	1.00000
.30	319.51	.92913	.98629	.99264	.86940	.93938	.86940
.60	639.01	.81013	.98556	.97582	.70070	.78393	.70070
.90	958.52	.68558	.96774	.95237	.54864	.59996	.54844
1.20	1278.03	.56962	.94421	.92381	.43110*	.42615	.43119*
1.50	1597.53	.46736	.91573	.89132	.34282	.30942	.34282
1.80	1917.04	.37992	.88330	.85549	.27623	.24517	.27623
2.10	2236.55	.30667	.84790	.81443	.22487	.21963	.22446
2.40	2556.05	.24615	.81042	.77969	.18419	.21066	.16419
2.70	2875.56	.19668	.77164	.74034	.15127	.22310	.15127
3.00	3195.06	.15655	.73226	.70091	.12422	.23031	.12422

FIGURE 8   EXAMPLE OF MODE-II OUTPUT FROM IONSCNT.   The temporal (lag shown in first column) and one-dimensional spatial (lag along drift direction of diffraction pattern shown in second column) autocorrelation functions of phase and intensity are shown in the fifth and eighth (rightmost) columns, respectively.   Other columns give similar information for the focus and scatter components of the scintillating signal, individually.   Geometrical information is given at the top.

LA-4259-44

31

FIGURE 9   VHF INTENSITY (S4) AND PHASE (PRMS) SCINTILLATION INDICES CALCULATED FOR A SATELLITE PASS OVER POKER FLAT, ALASKA, UNDER QUIET GEOMAGNETIC CONDITIONS. In this case, the scintillation enhancement after mid-pass is primarily a geometric effect stemming from propagation nearly along sheet-like irregularities supposed to be aligned along L-shells.
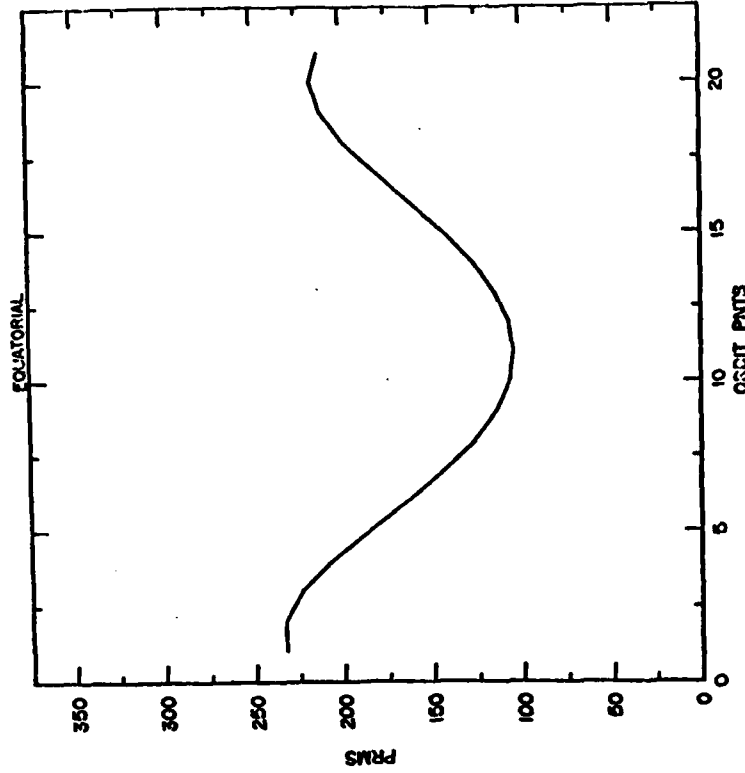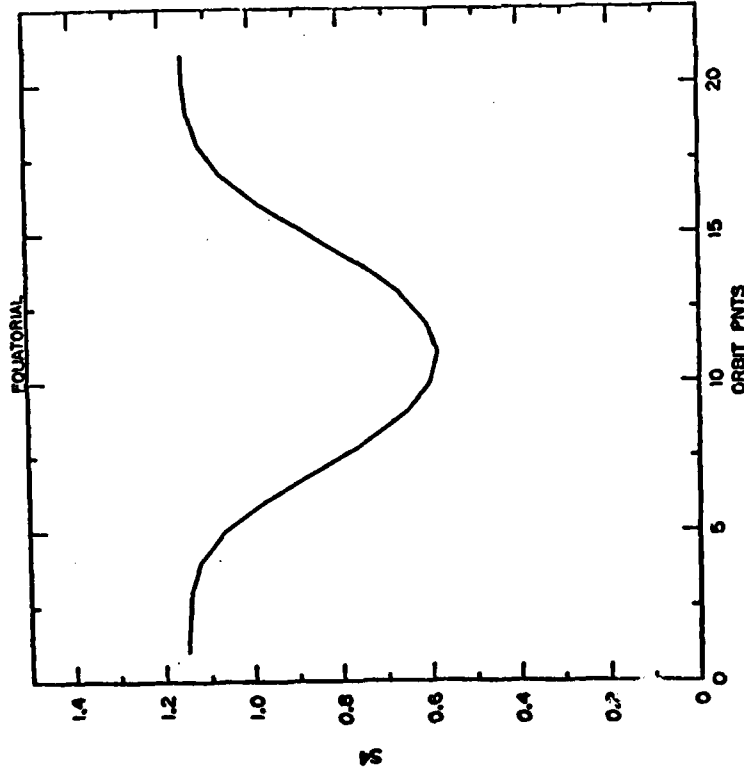
32

FIGURE 10   VHF INTENSITY (S4) AND PHASE (PRMS) SCINTILLATION INDICES CALCULATED FOR A NORTH-SOUTH
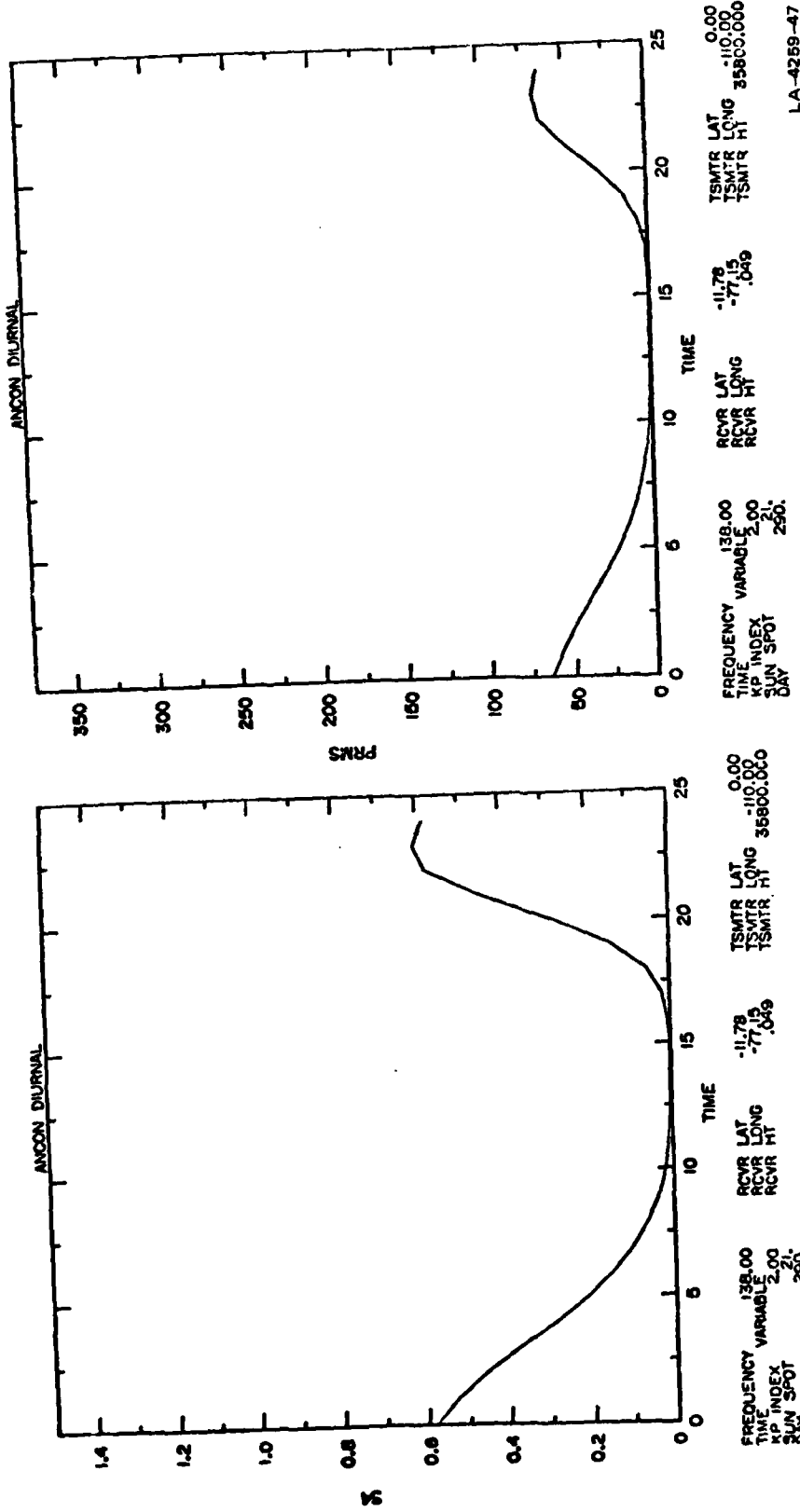SATELLITE PASS OVER ANCON, PERU, NEAR SOLAR MINIMUM

33

FIGURE 11   DIURNAL VARIATION OF VHF INTENSITY (S4) AND PHASE (PRMS) SCINTILLATION INDICES CALCULATED FOR OBSERVATION OF A GEOSTATIONARY SATELLITE FROM ANCON, PERU, IN OCTOBER OF A YEAR NEAR SOLAR MINIMUM. The user is cautioned that the phase scintillation calculated is that arising only from ionospheric irregularities with cross-field scale sizes on the order of a kilometer and smaller. Larger-scale trends also will contribute to the rms phase fluctuation measured over time scales greater than a few tens of seconds.
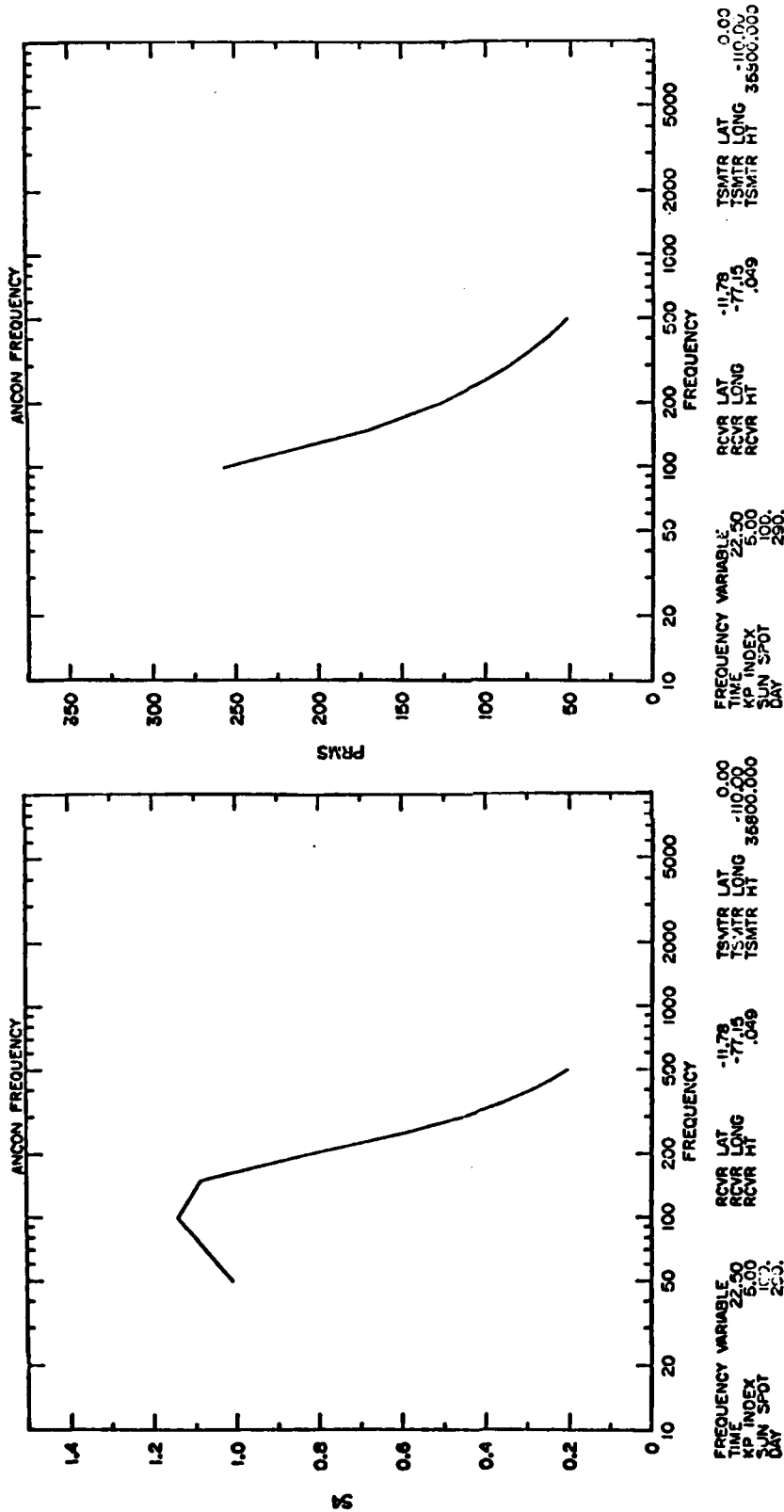
34
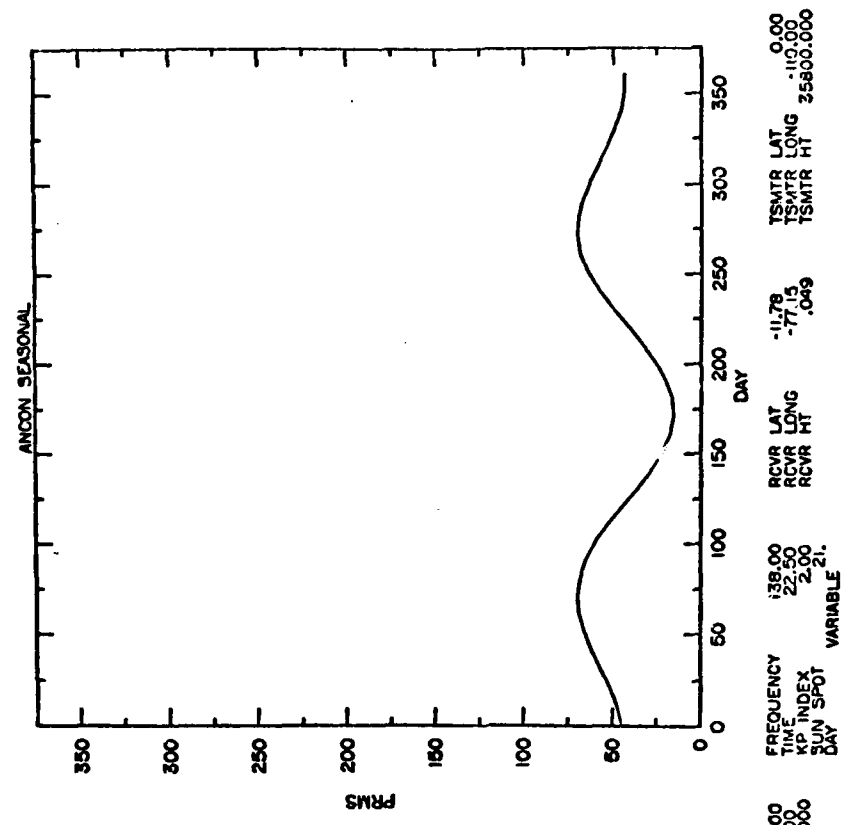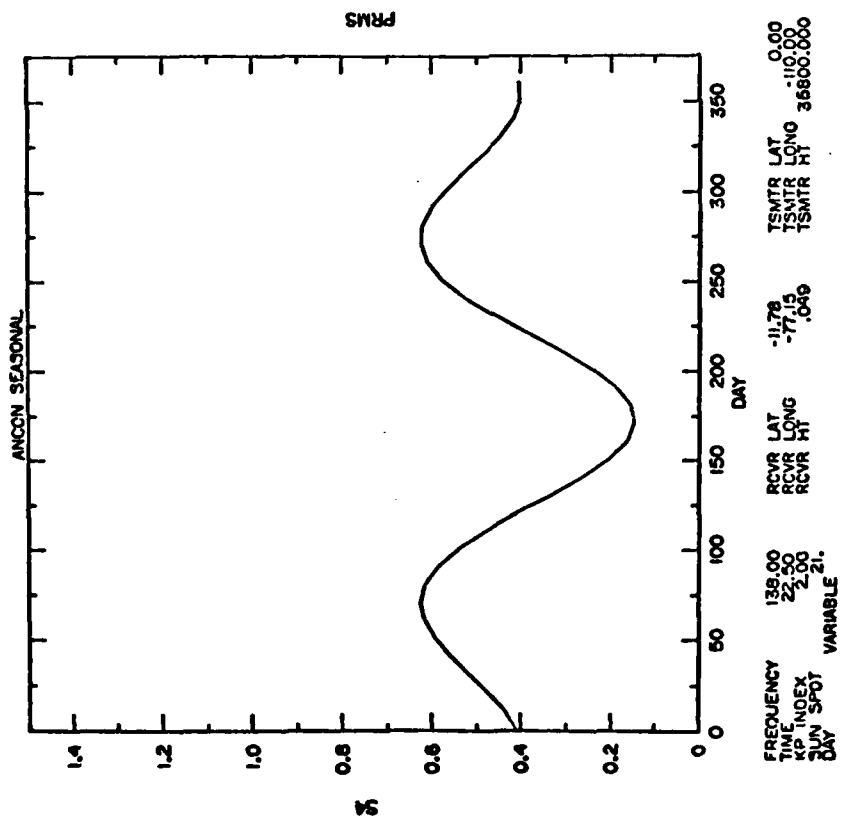
FIGURE 12   CALCULATED SEASONAL VARIATION OF NIGHTTIME SCINTILLATION AT ANCON NEAR SOLAR MINIMUM

LA-4259-48

35
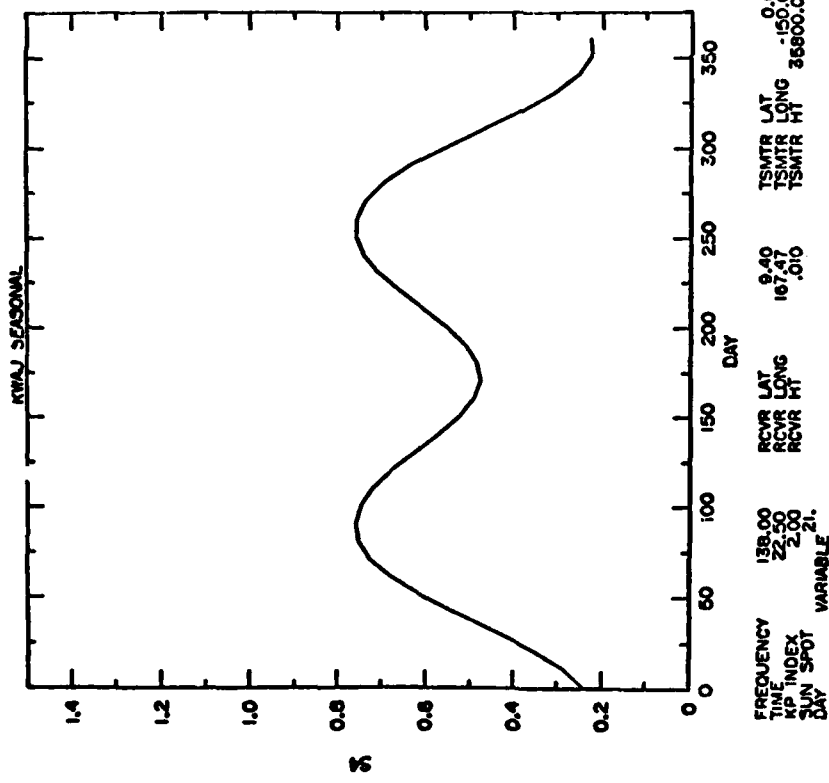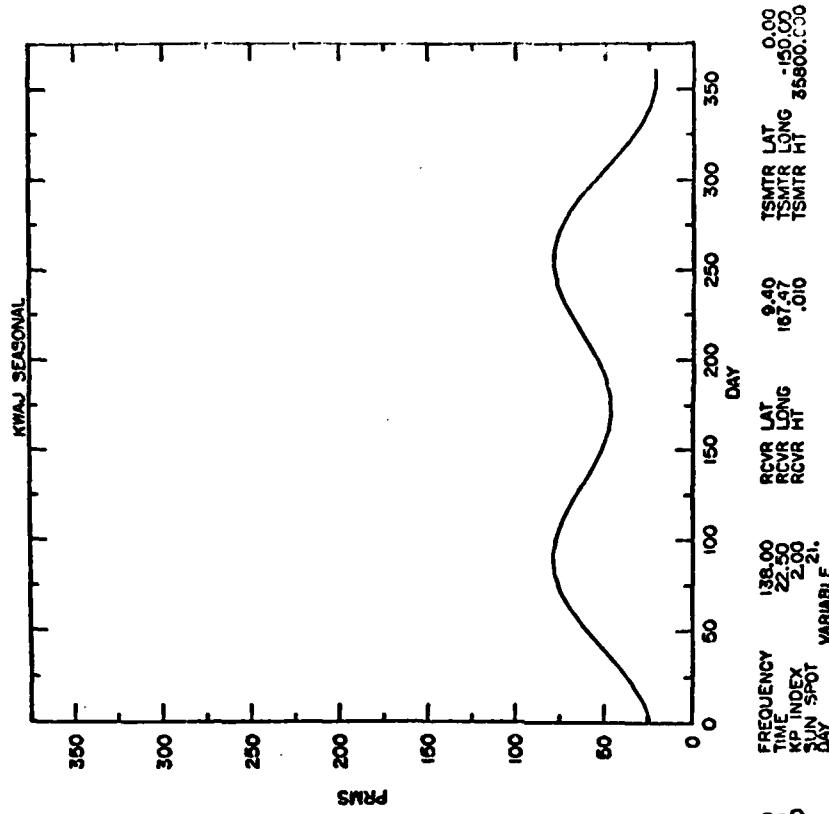
FIGURE 13 CALCULATED SEASONAL VARIATION OF NIGHTTIME SCINTILLATION AT KWAJALEIN, MARSHALL ISLANDS, NEAR SOLAR MINIMUM. Note differences near solstices compared with Figure 6.

36

FIGURE 14   CALCULATED FREQUENCY DEPENDENCE OF AVERAGE NIGHTTIME SCINTILLATION IN THE EQUATORIAL REGION NEAR AN EQUINOX DURING A YEAR OF ELEVATED SOLAR ACTIVITY. The code would predict Rayleigh statistics ($S_4 = 1.0$) under these conditions for frequencies below 50 MHz. The phase scintillation index (PRMS) varies approximately as f^{-1}.

37

signal-statistical model does permit values greater than unity in the presence of substantial focusing. The ray-optics approximation employed for calculating propagation of the focus component is not always fully satisfactory, and a limit on it has been incorporated in the code for conditions of strong scatter. It is to be noted that S_4 values up to 1.2 are observed occasionally, at least at VHF near the geomagnetic equator.

V CONCLUSION

This report and its companion volume (Rino et al., 1977) describing computer codes IONSCNT and DIST constitute the final reports on this contract to develop a transionospheric channel model. The work began as an attempt to collate previously existing and highly fragmented scintillation data into a form useful for system application. During the course of the work, however, both experimental and theoretical work on transionospheric radio propagation progressed considerably. The major experimental development was the advent of complex-signal data from coherent radio beacons on the Navy navigation (Transit) satellites ATS-6 and P76-5 (the DNA-002 wideband beacon). The theory of propagation in a random medium advanced both analytically and by application of numerical calculation to strong-scatter problems.

Availability of the coherent-beacon data has yielded much insight into the complex-signal statistics of scintillation, and this insight has been incorporated in our work to provide a signal-statistical model that is complementary to deterministic models of TEC effects. Our ability to incorporate the new experimental findings has been limited, however, by the theoretical framework we have employed. Signal-statistically, the most fundamental limitation of the present model is its heavy reliance on choice of an outer scale to describe scintillation-producing ionospheric structure. It is very likely that the outer scales invoked in the model (900 m in the equatorial region and 2.6 km elsewhere) have no geophysical significance; rather they represent the largest scales that contribute to intensity scintillation on the paths employed in collection of the data we used for quantitative calibration and iterative testing of the model. The paths employed were mainly between satellites in high-inclination, moderate-altitude (1000-km) orbits and the ground.

The main caution to be employed as a result of the outer-scale dilemma arises in application of the model to phase-sensitive systems where

39

long-term stability is important, especially in the equatorial region. The user must always keep in mind that the rms phase fluctuations described by the code are those produced by ionospheric structures on the order of a kilometer and smaller in east-west extent near the equator (30 km and smaller in north-south extent). Phase trends due to larger-scale structure must be accounted for separately. For geostationary systems, this translates into time scales substantially longer than 20 s.

Morphologically, the most important limitation of the model is that it does not account for night-to-night departures of scintillation conditions on a given communication link during the same season, at the same local time, and under the same solar and geomagnetic conditions, which can be substantial. The model describes only the "expectation level" of scintillation for a specified set of observing conditions. Data now being accumulated could be employed to include a description of departures from mean scintillation conditions, but the present model stops short of doing so. Mean morphological limitations of the model include some uncertainty over long-term trends in activity during a solar cycle and virtual absence of any data from the polar caps for use in establishing the model.

Despite the foregoing limitations, the model described in this report is the most extensive computer-coded assimilation of scintillation information presently available for systems planning. It will provide systems-relevant characterization of scintillation for a wide range of operating circumstances. Hopefully it also can serve as a baseline for analysis of existing and forthcoming scintillation data, in attempts to understand the nature and dynamics of ionospheric structure.

REFERENCES

Beckman, P., and A. Spizzichino, <u>The Scattering of Electromagnetic Waves from Rough Surfaces</u>, pp. 119-136 (Pergamon Press, New York, N.Y., 1963).

Bramley, E. N., "Some Aspects of the Rapid Directional Fluctuations of Short Radio Waves Reflected at the Ionosphere," <u>Proc. IEE</u>, Vol. 102, pp. 533-540 (1955).

Fremouw, E. J. and C. L. Rino, "Continued Modeling of Transionospheric Radio Propagation," Quarterly Technical Report 4, Contract F30602-75-C-0236, SRI Project 4259, SRI International, Menlo Park, Calif. (August 1976).

Fremouw, E. J., R. L. Leadabrand, R. C. Livingston, M. D. Cousins, C. L. Rino, B. C. Fair, and R. A. Long, "Early Results from the DNA Wideband Satellite Experiment--Complex-Signal Scintillation, submitted to <u>Radio Science</u> (1977).

Hatfield, V. E., and C. L. Rino, "Non-Rician Statistics and Their Implications for Modeling Effects of Scintillation on Communication Channels," in <u>The Effect of the Ionosphere on Space Systems and Communications</u>, J. M. Goodman, ed. (Naval Research Laboratory, Washington, D.C., January 1975).

Klobuchar, J. A., "A First-Order Worldwide, Ionospheric, Time-Delay Algorithm," Report AFCRL TR-75-0502, Air Force Cambridge Research Laboratory, Hanscom AFB, Mass. (September 25, 1975).

Koster, J. R., "Equatorial Studies of the VHF Signal Radiated by Intelsat II, F-3; 1. Ionospheric Scintillation," Progress Report No. 3. Contract No. F61052-67-C-0027, University of Ghana-Legon, Accra, Ghana (1966).

Koster, J. R., I. Katsriku, and M. Tete, "Studies of the Equatorial Ionosphere Using Transmissions from Active Satellites," Annual Summary Report 1, Contract AF61(052)-800, University of Ghana-Legon, Accra, Ghana (1966).

Ratcliffe, J. A., "Some Aspects of Diffraction Theory and Their Application to the Ionosphere," <u>Repts. Prog. Phys.</u>, Vol. XIX, pp. 188-207 (1956).

Rice, S. O., "Mathematical Analysis of Random Noise," Part III, <u>Bell Syst. Tech. J.</u>, Vol. 24, No. 1. pp. 47-159 (1945).

Rino, C. L., "Evidence of Sheet-Like Irregularity Structures in the Diffuse Aurora," paper to be presented at IAGA/IMAP Meeting, Seattle, Wash., August 22-September 3, 1977.

Rino, C. L., and E. J. Fremouw, "Statistics for Ionospherically Diffracted VHF/UHF Signals, Radio Science, Vo. 8, No. 3, pp. 223-233 (1973).

Rino, C. L., and E. J. Fremouw, "The Angle Dependence of Singly Scattered Wavefields," submitted to J. Atmos. Terr. Phys. (1977).

Rino, C. L., R. C. Livingston, and H. E. Whitney, "Some New Results on the Statistics of Radio Wave Scintillation 1. Empirical Evidence for Gaussian Statistics," J. Geophys. Res., Vol. 81, No. 13, pp. 2051-2057 (1976).

Rino, C. L., A. R. Hessing, V. E. Hatfield, and E. J. Fremouw, "A FORTRAN Program for Calculating Global Ionospheric Amplitude and Phase Scintillation," Quarterly Technical Report 8, Contract F30602-75-C-0236, SRI Project 4259, SRI International, Menlo Park, Calif. (July 1977).

Woodman, R. F., and C. La Hoz, "Radar Observations of F-Region Equatorial Irregularities," J. Geophys. Res., Vol. 81, No. 31, pp. 5447-5466 (1976).